This is a repository copy of *An improved airborne multichannel SAR imaging method with motion compensation and range-variant channel mismatch correction*.

White Rose Research Online URL for this paper:
http://eprints.whiterose.ac.uk/165806/

Version: Published Version

An Improved Airborne Multichannel SAR Imaging Method With Motion Compensation and Range-Variant Channel Mismatch Correction

Jiayi Guo ⃝, *Graduate Student Member, IEEE*, Jie Chen ⃝, *Senior Member, IEEE*, Wei Liu ⃝, *Senior Member, IEEE*, Chunsheng Li, and Wei Yang ⃝, *Associate Member, IEEE*

Abstract—To obtain a high-resolution and wide-swath image, the azimuth multichannel technique has been widely used in synthetic aperture radar (SAR) systems to overcome the contradiction between the wide swath and high pulse repetition frequency. For a high image quality, channel mismatch correction is an essential step in the multichannel SAR data imaging. However, in the case of airborne multichannel SAR, motion errors will severely degrade the performance of channel mismatch correction. To deal with this problem, this article proposes an improved airborne multichannel SAR imaging method with motion compensation, and range-variant channel mismatch correction. First, motion errors are compensated based on resampling and phase compensation. Then, the time-delay and constant gain-phase errors between channels are estimated and corrected, followed by the range-variant phase error correction based on a novel range-down-sampling method, which reduces the influence of motion errors on the channel mismatch correction significantly. Finally, simulated and real data processing results are used to demonstrate the effectiveness of the proposed method.

Index Terms—Channel mismatch estimation, motion compensation, multichannel, synthetic aperture radar (SAR).

I. INTRODUCTION

HIGH-RESOLUTION and wide-swath (HRWS) SAR image formation has a wide range of applications in both military and civilian fields [1]. Traditionally, HRWS cannot be obtained simultaneously due to the limitation of the pulse repetition frequency (PRF) [2], [3]. A low PRF is needed for wide-swath observation, while to realize the azimuth high resolution, the PRF should be high enough to avoid serious Doppler ambiguity. To overcome this contradiction, the azimuth multichannel SAR technique is developed [4]–[6], using a single channel for signal transmission and multiple channels to receive echoes simultaneously. By adding multiple receiving channels, the azimuth sampling rate is increased equivalently, and azimuth HRWS can be realized at the same time. However, with respect to arbitrary single channel data, azimuth spectrum is ambiguous, because PRF is low compared with Doppler bandwidth corresponding to main lobe width of the antenna. Therefore, construction of azimuth data with all receiving channel data is necessary for ambiguity-free Doppler spectrum via digital beam forming [6]–[9].

In order to guarantee a high image quality, some factors should be accounted for before the airborne multichannel SAR data reconstruction. One is the motion error of the platform, including along-track position error and line-of-sight (LOS) displacement error, i.e., cross-track position error, and the other is channel mismatch, including gain-phase and time-delay errors between channels. Furthermore, since channel characteristic changes along the range direction, the phase error between the channels also changes with the range, which should be taken into account during the estimation. These errors severely affect the accuracy of the azimuth spectrum reconstruction and degrade the image quality, including resolution loss and appearance of the ghost target. Therefore, before azimuth spectrum reconstruction, motion and channel mismatch errors should be compensated.

Many motion compensation (MOCO) methods have been studied in the airborne SAR imaging based on the extended chirp-scaling (ECS) algorithm to correct the LOS displacement error [10]. There are two steps in the ECS method, including range-invariant error compensation and range-variant error correction after range cell migration correction (RCMC). Moreover, to improve the accuracy of the motion error estimation and obtain a high-resolution image, the autofocus technique has been employed during MOCO [11]–[13]. However, the MOCO methods mentioned previously are only suitable for single-channel SAR data processing, with poor performance in the case of multichannel data processing. An improved two-step MOCO method for multichannel SAR is proposed in [14], which corrects the LOS displacement error of different channels, respectively. On this basis, the along-track position error is eliminated by resampling received data, which is adopted in this article.

After MOCO, the gain-phase and time-delay errors between channels should be corrected. An azimuth cross-correlation method is proposed in [15]–[17], which estimates the two

Jiayi Guo, Jie Chen, and Wei Yang are with the School of Electronic, and Information Engineering, Beihang University, Beijing 100191, China (e-mail: jiayiguo@buaa.edu.cn; chenjie@buaa.edu.cn; yangweigigi@sina.com).

Wei Liu is with the Department of Electronic, and Electrical Engineering, University of Sheffield, S10 2TN Sheffield, U.K. (e-mail: w.liu@sheffield.ac.uk).

Chunsheng Li is with the School of Electronic, and Information Engineering, Beihang University, Beijing 100191, China, and also with the Collaborative Innovation Center for Geospatial Information Technology, Wuhan 430079, China (e-mail: lics@buaa.edu.cn).

different errors with a simple operation. However, as for the phase error correction, the performance is dependent on the Doppler centroid frequency accuracy, and since the phase error is estimated at the range frequency domain, it cannot accommodate the range variance of the phase error effectively. Based on the spectrum power distribution, another phase error estimation method is presented by minimizing the leaked spectrum energy caused by the phase error [18]–[20]. However, the robustness of the method is relatively poor and it also has a high computational complexity, because it is sensitive to the Doppler centroid frequency error and characteristics of the scenes and an iterative operation is employed by this method. By adopting the multiple signal classification (MUSIC) technique, several advanced methods are developed [21]–[24], through extracting the signal subspace and noise subspace from the covariance matrix of the Doppler spectrum, and the orthogonality between subspaces is used to estimate the phase error. This method does not need to estimate the Doppler centroid frequency but requires that the Doppler ambiguity number is smaller than the number of receiving channels. Moreover, in order to guarantee image quality of the whole scene, the range-variant phase error is taken into account, which can be estimated by dividing data into blocks in range, and then, obtaining the phase error curve by fitting [25]–[27]. In [25], a minimum entropy-based algorithm is used to estimate channel phase errors of each block. However, the iterative numerical minimization procedure of this algorithm requires large computation. In [26], weighted least-squares fitting is used to get the channel position error, and then, range-variant phase errors are deduced, and it obtains azimuth-dependent phase errors by smoothing and interpolating estimates results along the azimuth direction, making the space-variant phase error calibration more accurate. However, the influence of motion errors on the channel mismatch estimation is not analyzed in these methods, which degrade the performance of the channel mismatch estimation significantly.

In this article, to deal with this problem, a novel method is proposed. First, motion errors are compensated before the coarse channel mismatch estimation, with along-track position error corrected by the azimuth resampling and the channel-dependent LOS displacement error corrected by method in [14]. Second, a novel range-down-sampling method is implemented before the range-variant channel phase error estimation. By range-down-sampling operation, not only the impact of residual motion errors is reduced, but also the data quantity is decreased, which makes the estimation more accurate and quickly compared with other range-variant channel phase mismatch correction methods. After the MOCO and channel mismatch correction, azimuth spectrum reconstruction and traditional chirp scaling (CS) imaging [28] can be performed to complete the image formation.

This article is organized as follows. In Section II, a signal model of the airborne multi-channel SAR is provided with an analysis of both motion errors and channel mismatch. In Section III, the motion compensation method and coarse channel mismatch correction method are discussed, and azimuth cross-correlation is performed in the range frequency domain to estimate the time-delay and constant gain-phase errors. In Section IV, the range-variant phase error estimation method
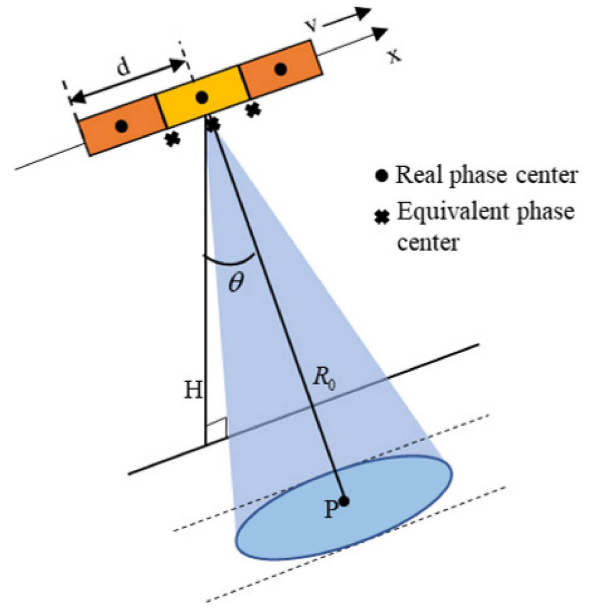

Fig. 1.   Operation geometry of the airborne multichannel SAR system.

is presented based on the MUSIC algorithm by dividing the data into subblocks. The novel range-down-sampling method is introduced, and the influence of the range sampling rate on the phase error estimation accuracy is analyzed in detail. In Section V, simulated data and real airborne SAR data are used to validate the proposed multichannel SAR imaging method. Finally, Section VI concludes this article.

II. Signal Model of Airborne Multichannel SAR

A. Ideal Signal Model of Airborne Multichannel SAR

The operation geometry of the airborne multichannel SAR system is shown in Fig. 1, where the X-axis is the flight direction, v is the platform velocity, d is the displacement interval of adjacent antenna phase centers, H denotes the platform height, R_0 is the shortest range between point target and transmit phase center, and θ is the incidence angle. In the multichannel SAR system, the middle channel transmits signals and all channels receive signals simultaneously. The echo of the channel i ($i = 0, 1, \ldots, I - 1$) at time t_k can be expressed as

$$
S_i(\tau, t_k) = \sigma \cdot W_a(t_k) \cdot \alpha \left(\tau - \frac{R(t_k) + R(t_k + \frac{x_i}{v})}{c} \right)
$$
$$
\cdot \exp \left(-j\pi b \left(\tau - \frac{R(t_k) + R(t_k + \frac{x_i}{v})}{c} \right)^2 \right)
$$
$$
\cdot \exp \left(-j\frac{2\pi}{\lambda} \left[R(t_k) + R\left(t_k + \frac{x_i}{v}\right) \right] \right) \quad (1)
$$

where τ and t_k denote the range fast time and azimuth slow time, b is the chirp rate, c is the light velocity, σ is the clutter reflectivity of the scatter point, x_i denotes the displacement between the phase center of the transmit channel (reference channel) and the phase center of the receive channel i, and $R(t_k)$ denotes the range between the transmit phase center and the target at
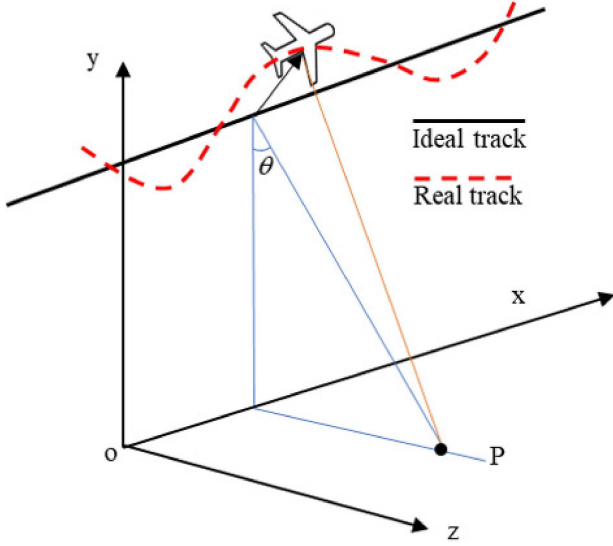
Fig. 2.   Trajectory deviation of airborne SAR.

Fig. 3.   LOS displacement in the cross-track plane.

the time t_k. By analyzing the range history, the equivalent slant range can be written as follows:

$$R(t_k) + R\left(t_k + \frac{x_i}{v}\right) \approx 2R\left(t_k + \frac{x_i}{2v}\right). \qquad (2)$$

Therefore, echo $S_i(\tau, t_k)$ is equivalent to self-transmitting and self-receiving data corresponding to the effective phase center at the middle of the transmitting phase center and receiving phase center [8], as shown in Fig. 1. The echo received by the ith channel is equivalent to the traditional single channel echo with a time delay $\frac{x_i}{2v}$ and down sampling. According to Fourier transform characteristics, the echo of the channel i in the azimuth frequency domain can be expressed as (for simplicity, assume that the Doppler ambiguity number is N, $N = 2M + 1$, $n = -M, -M + 1, ..., 0, 1, ..., M - 1, M$)

$$S_i(f) = \sum_{n=-M}^{M} S(f + n \cdot f_{\text{PRF}}) \cdot H_i(f + n \cdot f_{\text{PRF}})$$

$$f \in \left[-\frac{N}{2}f_{\text{PRF}}, -\frac{N}{2}f_{\text{PRF}} + f_{\text{PRF}}\right] \qquad (3)$$

where

$$H_i(f) = \exp\left\{+j\frac{x_i}{2v}2\pi f\right\} \qquad (4)$$

$S(f)$ denotes the azimuth spectrum of the ideal single channel echo, f denotes the Doppler frequency, f_{PRF} denotes real PRF of multichannel SAR, and I denotes the number of receiving channel. Usually the number of receiving channels is larger than the number of Doppler ambiguities.

B. Signal Model of Airborne Multichannel SAR With Motion Errors and Channel Mismatch

Due to the influence of atmosphere, the aircraft platform will deviate from ideal trajectory and introduce motion errors, which is illustrated in Fig. 2. The X-axis is the along-track direction and the Z-axis is the cross-track direction. The along-track position
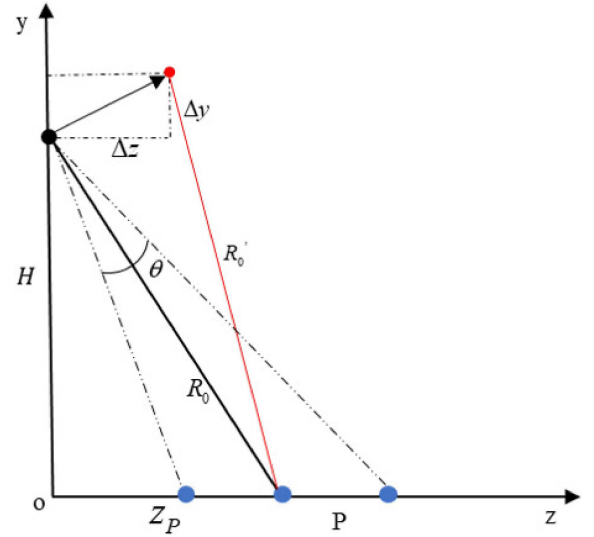
error is usually caused by velocity instability. The cross-track position error, also called LOS displacement, is shown in Fig. 3, where P is a point target in illuminated area with incidence angle θ. The displacement Δy along the Y-axis and Δz along the Z-axis can be acquired from inertial and global positioning system sensors onboard the aircraft. R_0 is the ideal shortest range between the sensor and target P, whereas R'_0 is the real range. Then, the LOS displacement error can be calculated as follows [10]:

$$\Delta r(\theta; t_k) = R'_0(\theta; t_k) - R_0(\theta)$$
$$\approx -\Delta z(t_k)\sin\theta + \Delta y(t_k)\cos\theta. \qquad (5)$$

Considering multiple channels, the LOS displacement error of different channels can be written as [14]

$$\Delta r_i(\theta; t_k) \approx -\Delta z(t_k)(\sin\theta_i + \sin\theta) + \Delta y(t_k)(\cos\theta_i + \cos\theta) \qquad (6)$$

where $\sin\theta_i = \frac{H \cdot \tan\theta}{\sqrt{R_0^2 + x_i^2}}$ and $\cos\theta_i = \frac{H}{\sqrt{R_0^2 + x_i^2}}$.

The channel mismatch includes the gain-phase and time-delay errors. As the phase error also changes with range [27], airborne multichannel SAR echoes of the channel i with motion errors and channel mismatch can be expressed as

$$S_i^1(\tau, t_k) = \sigma \cdot A_i \exp\{j\varphi_{i,\tau}\} \cdot W_a(t_k)$$
$$\cdot \alpha\left(\tau - \Delta\tau_i - \frac{2R(t_k + \frac{x_i}{2v}) + \Delta r_i(\theta; t_k)}{c}\right)$$
$$\cdot \exp\left(-j\pi b\left(\tau - \Delta\tau_i - \frac{2R(t_k + \frac{x_i}{2v}) + \Delta r_i(\theta; t_k)}{c}\right)^2\right)$$
$$\cdot \exp\left(-j\frac{2\pi}{\lambda}\left[2R(t_k + \frac{x_i}{2v}) + \Delta r_i(\theta; t_k)\right]\right) \qquad (7)$$

where A_i is the gain error, $\varphi_{i,\tau}$ is the phase error, including constant phase and range-variant phase errors, and $\Delta\tau_i$ is time-delay error.
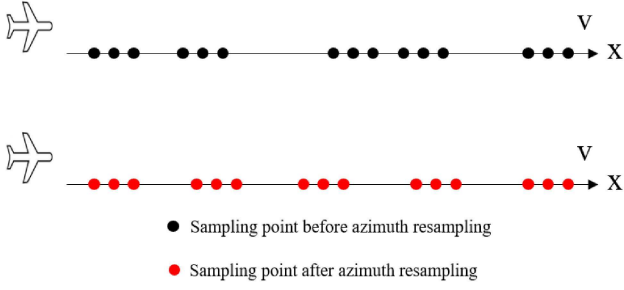
Fig. 4. Azimuth resampling process.

III. Motion Compensation and Coarse Channel Mismatch Correction

Since motion errors reduce the accuracy of the channel mismatch estimation severely, in this section, MOCO is performed first. The along-track position error and LOS displacement error are corrected by resampling and phase compensation, respectively. After that, time-delay and constant gain-phase errors are estimated and corrected by azimuth cross correlation.

Ignoring the range-variant phase error temporarily, and transforming (7) into the range frequency domain using the Fourier transform, we have

$$
\begin{aligned}
S_i^1(f_\tau, t_k) &= A_i \exp\{j\varphi_i\} S_i(f_\tau, t_k) \\
&\quad \cdot \exp\{-j2\pi f_r \Delta\tau_i\} \\
&\quad \cdot \exp\left\{\frac{-j2\pi(f_0 + f_\tau)\Delta r_i(\theta; t_k)}{c}\right\}
\end{aligned} \tag{8}
$$

where f_τ is range frequency, f_0 is carrier frequency, and $S_i(f_\tau, t_k)$ is the ideal echo of the channel i in the range frequency domain. According to (8), the LOS displacement error $\Delta r_i(\theta; t_k)$, time-delay error $\Delta\tau_i$, and constant gain-phase error $A_i \exp\{j\varphi_i\}$ need to be corrected before imaging.

A. Motion Compensation for Multichannel SAR Data

As mentioned, motion errors include both along-track position and LOS displacement errors. Usually the former is caused by the variation of the velocity and reduces the image quality significantly. Fig. 4 shows the process of receiving echoes of a three-channel SAR, where each circle represents a sampling point. Black circles denote the real sampling points, which are nonuniform, while red circles denote sampling points after azimuth resampling, which can be realized by interpolation based on the motion information acquired from inertial and global positioning system sensors.

The LOS displacement error $\Delta r_i(\theta; t_k)$ changes with the incidence angel θ so it is range variant. In this part, the range-invariant LOS displacement error $\Delta r_i(\theta_c; t_k)$ is used to replace the range-variant error, where θ_c is the central incidence angel. The range-invariant and channel-dependent motion error can be corrected in the range frequency domain by multiplying

$$
H_1(f_\tau, t_k) = \exp\left\{j2\pi(f_0 + f_\tau)\frac{\Delta r_i(\theta_c; t_k)}{c}\right\}. \tag{9}
$$

Ignoring residual range-variant motion errors, the echo of the channel i after motion compensation can be expressed as

$$
S_i^2(f_\tau, t_k) = A_i \exp\{j\varphi_i\} S_i(f_\tau, t_k) \exp\{-j2\pi f_r \Delta\tau_i\}. \tag{10}
$$

Note that residual range-variant motion errors still affect the phase error estimation result. In coarse channel mismatch correction, this effect is ignored. There are two reasons: first, after MOCO, the phase biases caused by residual range-variant motion errors only varies in the range of few degrees; and second, the coarse channel mismatch estimation method is performed in the range-frequency azimuth-time domain, and during this process, the data are averaged along the azimuth direction, which further reduces the influence of residual motion errors, as shown in Section III-B. The next range-variant phase error estimation is performed in the azimuth-frequency domain and need to be more accurate, so residual motion errors should be considered in this process. The range-down-sampling method is implemented to eliminate the influence of residual motion errors, which will be described in detail in Section IV.

B. Coarse Channel Mismatch Correction for Multichannel SAR Data

In this part, time-delay and constant gain-phase errors between channels are estimated and corrected. According to the properties of the Fourier transform, the time delay along the range is represented by a liner phase term in the range frequency domain. Using the first channel (channel 0) as the reference, the time-delay error between the channel i and the reference channel can be described as (11) by the azimuth cross-correlation and phase extraction operation [16].

$$
\Delta\tau_i = \frac{1}{2\pi} \cdot \frac{d\left(\arg\left(E_{t_k}\left(S_o^{*2}(f_\tau, t_k) \cdot S_i^2(f_\tau, t_k)\right)\right)\right)}{df_\tau} \tag{11}
$$

where $[]^*$ denotes a complex conjugate operation and E_{t_k} denotes expectation of the azimuth time t_k. The constant phase error between the channels i and 0 can be expressed as

$$
\varphi_i = E_{f_\tau}\left(\arg\left(E_{t_k}\left(S_o^{*2}(f_\tau, t_k) \cdot S_i^2(f_\tau, t_k)\right)\right) - 2\pi f_\tau \Delta\tau_i\right) - 2\pi f_{dc}\frac{x_i}{2v} \tag{12}
$$

where f_{dc} is the Doppler centroid frequency. It should be noted that when there is a Doppler centroid frequency error, the estimated result will not be accurate enough. However, the range-variant phase error will be estimated next and the residual phase error caused by the Doppler centroid frequency can be compensated effectively. The gain error can be represented by

$$
A_i = E_{f_\tau, t_k}\left(\frac{|S_i^2(f_\tau, t_k)|}{|S_0^2(f_\tau, t_k)|}\right). \tag{13}
$$

Multiplying (10) with the following correction function (14), the time-delay error and constant gain-phase error can then be corrected.

$$
H_2(f_\tau, t_k) = \exp\{j2\pi f_r \Delta\tau_i\} \exp\{-j\varphi_i\} A_i. \tag{14}
$$

TABLE I
PHASE ERROR ESTIMATION RESULTS UNDER DIFFERENT CONDITION

Channel mismatch in phase(degree)	Channel 1	Channel 2	Channel 3	Channel 4	Channel 5	Channel 6
Real phase error	0	30	24	24	10	5
Azimuth cross correlation [16]	0	30.04	24.08	22.19	8.66	3.92
Estimated deviation	0	0.04	0.08	1.81	1.34	1.08
Azimuth cross correlation with range-down-sampling	0	30.02	24.07	23.61	9.61	4.99
Estimated deviation	0	0.02	0.07	0.39	0.39	0.01
MUSIC [21]	0	29.33	23.33	23.36	9.25	3.24
Estimated deviation	0	0.67	0.67	0.64	0.75	1.76
MUSIC with range-down-sampling	0	29.97	24.50	24.13	10.13	5.24
Estimated deviation	0	0.03	0.50	0.13	0.13	0.24

IV. RANGE-VARIANT PHASE ERROR ESTIMATION BASED ON RANGE DOWN SAMPLING AND BLOCK PROCESSING

In this section, the range-variant phase error is estimated and compensated. To reduce the effect of noise and residual motion errors, range down sampling is adopted. The influence of range-down-sampling on the phase error estimation result is analyzed first. Then, a range-variant phase error estimation method based on the MUSIC algorithm is presented with range down sampling.

A. Influence of Range Down Sampling on Phase Error Estimation

Taking residual motion errors $\Delta r_i{}'(\theta; t_k)$ into consideration, multichannel echo after the motion compensation and coarse channel mismatch correction can be expressed as

$$S_i{}^3(f_\tau, t_k) = S_i(f_\tau, t_k) \exp\left\{ \frac{-j2\pi(f_0 + f_\tau)\Delta r_i'(\theta; t_k)}{c} \right\} \tag{15}$$

where $S_i(f_\tau, t_k)$ denotes the echo with a residual range-variant phase error of the channel i in the range frequency domain. Assume that the range bandwidth is B_r, and the corresponding range resolution is $\rho_r = \frac{c}{2B_r}$. In airborne SAR, the smaller the ratio of motion error $\Delta r_i'(\theta; t_k)$ to resolution ρ_r, the smaller the influence of motion error is. Reducing the range bandwidth by range down sampling, the effect of motion errors will be reduced, which makes the phase error estimation more accurate.

Simulated data are used to validate the effectiveness of range down sampling. Phase and motion errors are added to the simulated six-channel airborne SAR data. The azimuth cross-correlation and MUSIC methods are used to estimate the phase error between channels. During processing, range down sampling is employed and the estimation results are shown in Table I. The estimated deviation of the channel phase error is defined as

$$\Delta\varphi = |\varphi - \hat{\varphi}| \tag{16}$$

where φ is real phase error and $\hat{\varphi}$ is estimated phase.

From Table I, it can be seen that estimated deviation is less than 2without range down sampling for both azimuth cross-correlation method and MUSIC method. After range down sampling, estimated deviation is less than 0.5. The accuracy of estimated results improves clearly. It can be concluded that motion errors affect the channel mismatch estimation performance

and the proposed range-down-sampling method can mitigate this effect.

B. Phase Error Estimation Based on the MUSIC Algorithm

Rewriting the echo signal of the channel i as follows:

$$S_i(\tau, f) = \exp\{j\Delta\delta_i\} \sum_{n=-M}^{M} S(\tau, f + n \cdot f_{\text{PRF}})$$
$$\cdot \exp\left\{ +j\frac{x_i}{2v}2\pi(f + n \cdot f_{\text{PRF}}) \right\} \tag{17}$$

where δ_i is the phase error related to the reference channel 0. Then, the echo matrix can be written as

$$\mathbf{T} = \mathbf{\Gamma P S} + \mathbf{n} \tag{18}$$

where

$$\mathbf{T} = \begin{bmatrix} S_0(\tau, f) \\ \vdots \\ S_i(\tau, f) \\ \vdots \\ S_{I-1}(\tau, f) \end{bmatrix} \tag{19}$$

$$\mathbf{\Gamma} = \begin{bmatrix} e^{j\delta_0} \cdots 0 \\ \vdots \ddots \vdots \\ 0 \cdots e^{j\delta_{I-1}} \end{bmatrix} \tag{20}$$

and

$$\mathbf{P} = \begin{bmatrix} e^{j2\pi\frac{x_0}{2v}(f - Mf_p)} \cdots e^{j2\pi\frac{x_0}{2v}(f + Mf_p)} \\ \vdots \ddots \vdots \\ e^{j2\pi\frac{x_{I-1}}{2v}(f - Nf_p)} \cdots e^{j2\pi\frac{x_{I-1}}{2v}(f + Nf_p)} \end{bmatrix} \tag{21}$$

is the steering matrix

$$\mathbf{S} = \begin{bmatrix} S(\tau, f - Mf_p) \\ \vdots \\ S(\tau, f) \\ \vdots \\ S(\tau, f + Mf_p) \end{bmatrix} \tag{22}$$

$$\mathbf{n} = \begin{bmatrix} n_0(\tau, f) \\ \vdots \\ n_i(\tau, f) \\ \vdots \\ n_{I-1}(\tau, f) \end{bmatrix} \tag{23}$$

is the noise vector, which is assumed to be independent of the signal.

The covariance matrix of the multichannel echo vector $\mathbf{T}$ is

$$\mathbf{R}(f) = E\left[\mathbf{TT}^H\right] = \mathbf{\Gamma P} E\left[\mathbf{SS}^H\right] \mathbf{P}^H \mathbf{\Gamma}^H + \sigma_n^2 \Sigma_0 \tag{24}$$

where $E[\bullet]$ represents the statistical expectation operation of τ, $[\bullet]^H$ denotes Hermitian transpose, σ_n^2 is noise power, and Σ_0 is the I-dimensional identity matrix. The eigendecomposition of the covariance matrix $\mathbf{R}(f)$ is given by

$$\mathbf{R}(f) = \sum_{i=0}^{N-1} \alpha_i u_i u_i^H + \sum_{i=N}^{I} \alpha_i u_i u_i^H \tag{25}$$

where $\alpha_0 > \alpha_1 > \cdots > \alpha_{N-1} \gg \alpha_N = \alpha_{N+1} = \cdots = \alpha_I = \sigma_n^2$ are the eigenvalues and u_i is the corresponding eigenvector. The signal subspace and noise subspace can be written as

$$\mathbf{U}_s = [u_0, u_1, \ldots, u_{N-1}] \tag{26}$$

$$\mathbf{U} = [u_N, u_{N+1}, \ldots, u_{I-1}]. \tag{27}$$

The signal subspace has the same span as the subspace constructed by the steering matrix $[\mathbf{\Gamma P}_{-M} \ldots \ldots, \mathbf{\Gamma P}_{+M}]$.

Based on the principle of the MUSIC algorithm [21], the noise subspace is orthogonal to the signal subspace, and the estimation of the phase error Γ is equivalent to solving the following equation:

$$\begin{aligned} \min_{\Gamma} J &= \min_{\Gamma} \left\{ \sum_{n=-M}^{+M} \left\| \mathbf{U}^H \mathbf{\Gamma P}_n \right\| \right\} \\ &= \min_{\Gamma} \left\{ \sum_{n=-M}^{+M} \mathbf{P}_n^H \mathbf{\Gamma}^H \mathbf{U} \mathbf{U}^H \mathbf{\Gamma P}_n \right\} \\ &= \min_{\Gamma} \left\{ x^H \sum_{n=-M}^{+M} \mathbf{Q}_n^H \mathbf{U} \mathbf{U}^H \mathbf{Q}_n x \right\} \end{aligned} \tag{28}$$

where $x = [e^{j\delta_0}, \ldots, e^{j\delta_{I-1}}]^T$ and $\mathbf{Q}_i = \text{diag}\{\mathbf{P}_n\}$. Then, the phase error estimation can be written as

$$\hat{x} = \frac{\mathbf{Z}^{-1} \mathbf{w}}{\mathbf{w}^T \mathbf{Z}^{-1} \mathbf{w}} \tag{29}$$

where $\mathbf{Z} = \sum_{n=-M}^{+M} \mathbf{Q}_n^H \mathbf{U} \mathbf{U}^H \mathbf{Q}_n$ and $\mathbf{w} = [1, 0, \ldots, 0]^T$, which means the channel 0 is the reference channel.

C. Range-Variant Phase Error Estimation

First range compression and range down sampling are operated in the range frequency domain. After that inverse FFT is taken along the range frequency. The range-time domain and azimuth-frequency domain echo of the channel i can be
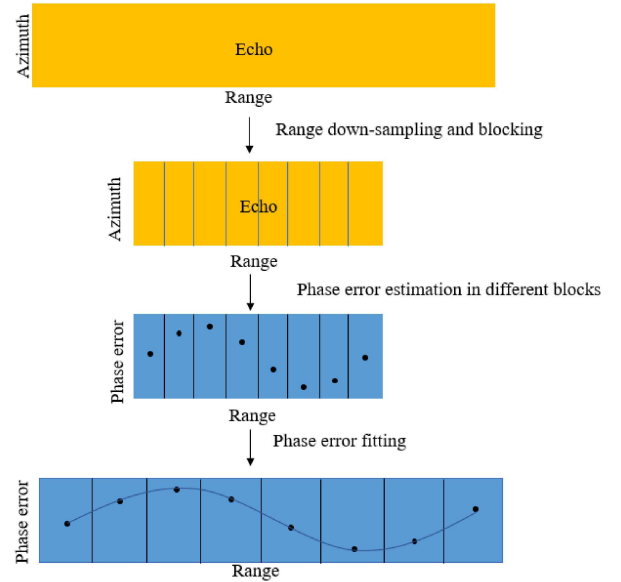

Fig. 5. Flowchart of the proposed range-variant phase error estimation process.

written as

$$S_i^3(\tau, f) = \exp\{j\Delta\delta_i(\tau)\} \sum_{n=-M}^{M} S(\tau, f + n \cdot f_{\text{PRF}}) \\ \cdot \exp\left\{+j\frac{x_i}{2v} 2\pi(f + n \cdot f_{\text{PRF}})\right\} \tag{30}$$

where $\Delta\delta_i(\tau)$ is the range-variant phase error. The data are divided into K blocks along the range. As phase error change slowly along the range, so it can be regarded as constant in each block, and the corresponding phase error of the block k is estimated as

$$\hat{x_k} = \frac{\mathbf{Z}_k^{-1} \mathbf{w}}{\mathbf{w}^T \mathbf{Z}_k^{-1} \mathbf{w}} \tag{31}$$

where $\mathbf{Z}_k = \sum_{n=-M}^{+M} \mathbf{Q}_n^H \mathbf{U}_k \mathbf{U}_k^H \mathbf{Q}_n$, $\mathbf{U}_k$ is the noise subspace of the block k after range down sampling. All the data in a block are used to calculate the covariance matrix and the noise subspace. The range-variant phase error of each channel is fitted with a polynomial using the estimated values [27], and the continuously changing phase error is obtained subsequently. The flowchart of the proposed processing is shown in Fig. 5.

After the range-variant phase error estimation and correction, channel mismatch correction is finished and azimuth spectrum can be reconstructed more accurately. The traditional CS SAR imaging method is then used and final imaging result of multichannel SAR data can be obtained. Fig. 6 shows a flow chart of the proposed airborne multichannel SAR imaging method.

V. EXPERIMENTAL RESULTS

A. Simulated Data

Simulations are carried out to validate the proposed method. The parameters are given in Table II. The errors analyzed in this article include motion errors, time-delay error, constant gain-phase error, and range-variant phase error. To validate the proposed phase error estimation method, point target simulation
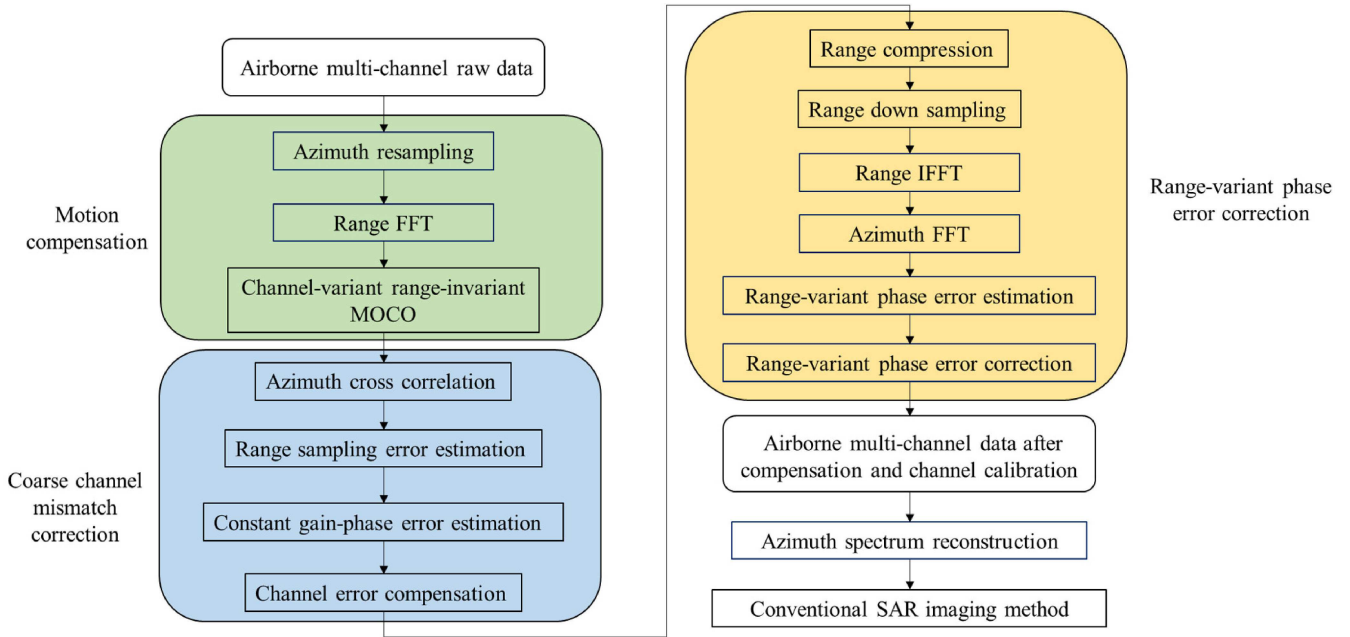
Fig. 6.   Flowchart of the proposed airborne multichannel SAR imaging method.

TABLE II
PARAMETERS OF THE SIMULATED AIRBORNE MULTICHANNEL SAR SYSTEM

Parameters	Values	Parameters	Values
Wavelength	0.03m	Azimuth Bandwidth	1097Hz
Bandwidth	180MHz	Velocity	185m/s
Sample rate	216MHz	Channel interval	0.2m
PRF	659Hz	Channel number	3

Fig. 7.   Azimuth profile of a point target corrected by different methods.

experiment is carried out. The range-variant phase error changes with incidence angle, however, for the arbitrary point target, the incidence angle is constant. Therefore, only constant phase error and motion errors are added to simulated data. Phase errors are set by adding a constant phase offset to the echo of each channel, which are $0°$, $30°$, and $10°$ in this experiment. Motion errors are set by adding position errors within 5 cm into the platform. Estimated results of the phase error using the traditional MUSIC algorithm are $0°$, $31.2°$, and $12.4°$ while estimated results by the proposed range-down-sampling method are $0°$, $29.7°$, and $10.5°$. The estimation accuracy is obviously improved by range down sampling. Fig. 7 shows azimuth profiles of a point target, which are corrected using two the aforementioned estimated phase errors, respectively. The false targets are obviously suppressed after the phase error correction. With range down sampling, false targets are further suppressed as the estimated phase error is more accurate.

B. Real Data

In this section, real airborne multichannel SAR data are used to validate the proposed method. The scene includes land, marine area, and island. The SAR system works in side-looking
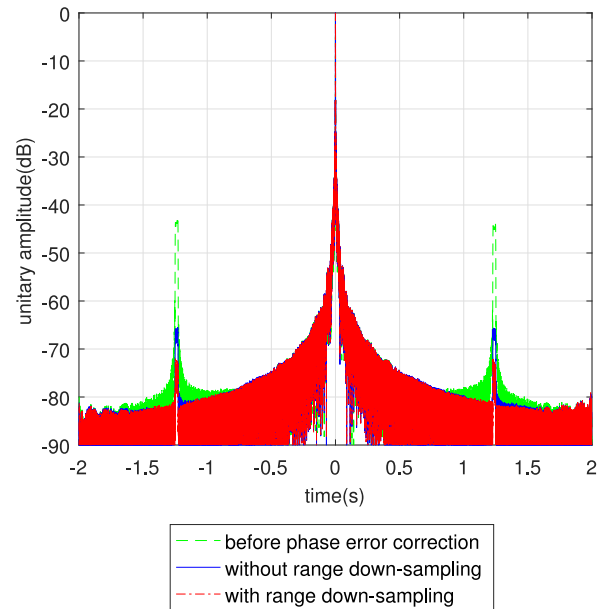
Stripmap mode with four channels distributed along the azimuth direction. The data are processed by the imaging method presented in this article as shown in Fig. 6. To compensate motion errors and correct channel mismatch, there are three key steps during processing schedule: motion compensation, coarse channel mismatch correction, and range-variant phase error correction. Imaging results after each step are shown and analyzed as follows.

1) Key Step 1 Motion Compensation: The data are processed by the MOCO method given in Section III-A. Fig. 8(a) is imaging
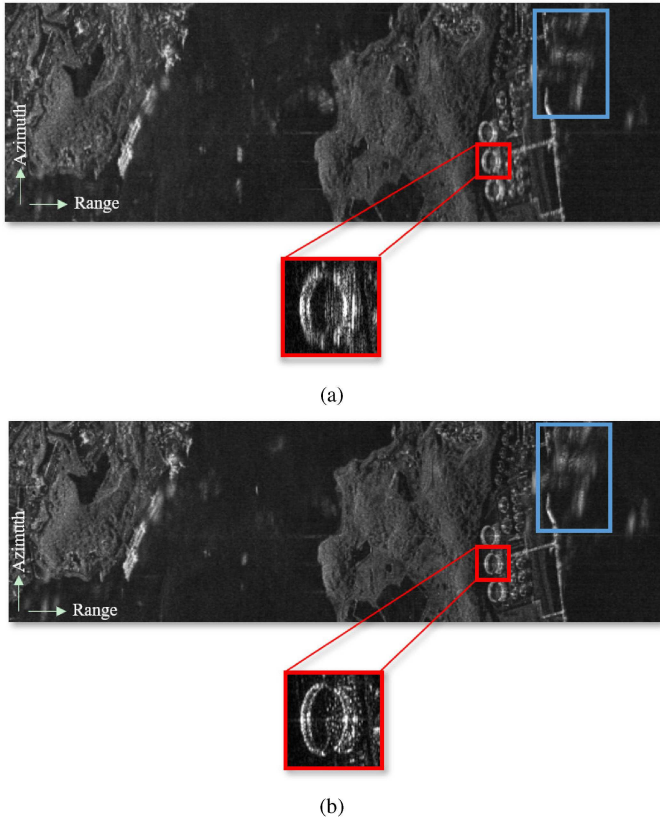
(a)

(b)

Fig. 8. Imaging results (a) without MOCO and channel mismatch correction, and (b) with MOCO without channel mismatch correction.
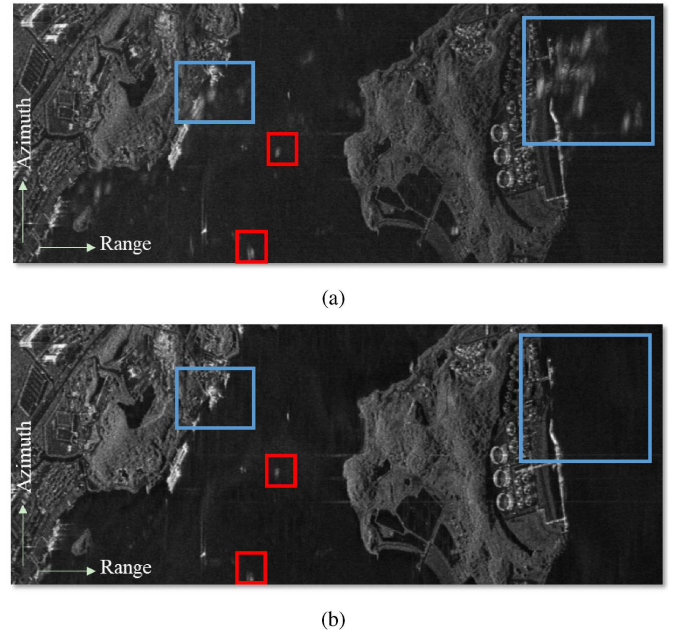

(a)

(b)

Fig. 9. Imaging results (a) without channel mismatch correction, and (b) with coarse channel mismatch correction.

Fig. 10. Range-variant phase error of different channels.

result without MOCO and channel mismatch correction. As motion errors exist, the image is seriously defocused, and there are false targets presents due to channel mismatch, as marked by the blue rectangle. Fig. 8(b) shows imaging result with MOCO. Compared with Fig. 8(a), Fig. 8(b) is better focused. However, false targets still exist because of the channel mismatch as shown in the blue rectangle.

2) Key Step 2 Coarse Channel Mismatch Correction: After MOCO, coarse channel mismatch is estimated and corrected. Time-delay and constant gain-phase errors are calculated by (11)–(13) and compensated by (14). Fig. 9(b) shows imaging result with coarse channel mismatch correction, while for convenience of comparison, Fig. 8(b) has been redisplayed in Fig. 9(a), which shows the result without channel mismatch correction. Compared with Fig. 9(a), false targets are effectively suppressed and the image is much clearer in Fig. 9(b), as marked by blue rectangles. However, there are still residual false targets, as marked by red rectangles. There are two main reasons. First, the estimated results of the phase error are not accurate enough because of residual motion errors and Doppler centroid frequency error. Second, range-variant phase error between channels still exists and has not been compensated yet.

3) Key Step 3 Range-Variant Phase Error Correction: Range-variant phase error is estimated according to method proposed in Section IV-C. After range down sampling, the data are divided into 16 blocks and the residual phase error is calculated in each block. Fig. 10 shows range-variant phase
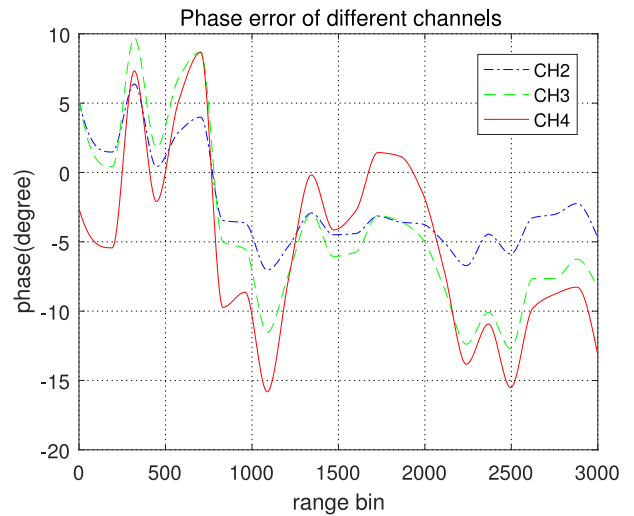
error for each range bin after fitting operation. Channel 1 is set as reference in the estimation.

Fig. 11(b) shows the imaging result after the range-variant phase error correction. Fig. 11(a) is the result with the constant phase error correction only. Clearly the false targets have been further suppressed, as shown by the blue rectangle.

4) Range-Down-Sampling Method Validation: To validate the range-down-sampling method, the range-variant phase error is estimated with range down sampling and without range down sampling separately. Fig. 12(a) is the result without range down sampling and Fig. 12(b) is with range down sampling. In Fig. 12(a), there are still some light false targets presents that are marked with blue rectangles, while in Fig. 12(b), these
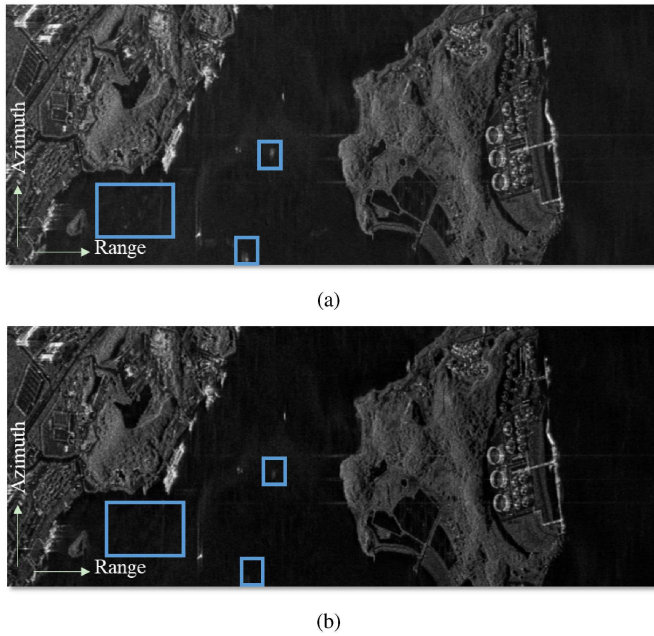
Fig. 11.   Imaging results (a) without range-variant phase error correction and (b) with range-variant phase error correction.
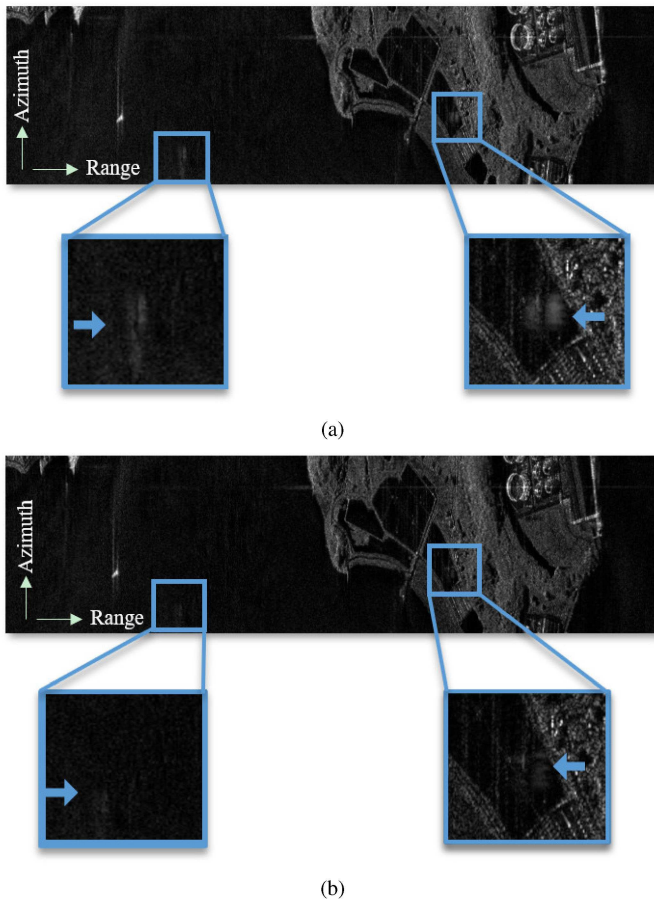

Fig. 12.   Imaging results (a) without range-down-sampling method and (b) with range-down-sampling method.

false targets are suppressed further, clearly demonstrating the effectiveness of the range-down-sampling operation. From these experimental results, the following can be found.

1) Motion compensation is essential for airborne multichannel SAR imaging, as motion errors not only cause a defocused image, but also reduce the accuracy of channel mismatch estimation and azimuth spectrum reconstruction.

2) After time-delay and constant gain-phase errors correction, most false targets are suppressed, however, due to residual range-variant phase error and residual motion errors, there are still some lights false targets presents in the image.

3) By range down sampling, the range-variant phase error can be estimated more accurately.

VI. CONCLUSION

An improved airborne multichannel SAR imaging method based on motion compensation and range-variant channel mismatch correction has been proposed in this article. Motion errors and channel mismatch are corrected in three key steps. First, motion compensation is performed to correct along-track position error and LOS displacement error. Next, time-delay error and constant gain-phase error between channels are estimated using azimuth cross-correlation method and coarse channel mismatch correction is accomplished. Finally, the range-variant phase error is estimated using the MUSIC algorithm with range down sampling. The effect of range-down sampling on the phase error estimation is analyzed, showing that by range down sampling, the influence of the residual motion error is reduced and the accuracy of estimation is improved. The effectiveness of the proposed method has been demonstrated by experimental results based on both simulated and real data.

REFERENCES

[1] A. Moreira, P. Prats-Iraola, M. Younis, G. Krieger, I. Hajnsek, and K. P. Papathanassiou, "A tutorial on synthetic aperture radar," *IEEE Geosci. Remote Sens. Mag.*, vol. 1, no. 1, pp. 6–43, Apr. 2013.

[2] J. Curlander and R. McDonough, *Synthetic Aperture Radar: Systems and Signal Processing*. New York, NY, USA: Wiley, 1991.

[3] A. Currie and M. A. Brown, "Wide-swath SAR," *IEE Proc. F—Radar Signal Process.*, vol. 139, no. 2, pp. 122–135, Apr. 1992.

[4] G. D. Callaghan and I. D. Longstaff, "Wide-swath space-borne SAR using a quad-element array," *IEE Proc. —Radar, Sonar, Navigat.*, vol. 146, no. 3, pp. 159–165, Jun. 1999.

[5] M. Suess, B. Grafmueller, and R. Zahn, "A novel high resolution, wide swath SAR system," in *Proc. IEEE Int. Geosci. Remote Sens. Symp.*, Sydney, NSW, Australia, 2001, pp. 1013–1015, doi: 10.1109/IGARSS.2001.976731.

[6] G. Krieger, N. Gebert, and A. Moreira, "Unambiguous SAR signal reconstruction from nonuniform displaced phase center sampling," *IEEE Geosci. Remote Sens. Lett.*, vol. 1, no. 4, pp. 260–264, Oct. 2004.

[7] G. Krieger, N. Gebert, and A. Moreira, "SAR signal reconstruction from non-uniform displaced phase centre sampling," in *Proc. IEEE Int. Geosci. Remote Sens. Symp.*, 2004, vol. 3, pp. 1763–1766.

[8] Wang Pengbo, Zhou Yinqing, Chen Jie, and Li Chunshen, "Multi-channel chirp scaling algorithm for high-resolution multi-channel antenna spaceborne SAR imaging," *J. Beijing Univ. Aeronaut. Astronaut.*, vol. 32, no. 4, pp. 440–444, 2006.

[9] F. Q. D. Almeida, M. Younis, G. Krieger, and A. Moreira, "A new slow PRI variation scheme for multichannel SAR high-resolution wide-swath imaging," in *Proc. Int. Geosci. Remote Sens. Symp.*, 2018, pp. 3655–3658.

[10] A. Moreira and Yonghong Huang, "Airborne SAR processing of highly squinted data using a chirp scaling approach with integrated motion compensation," *IEEE Trans. Geosci. Remote Sens.*, vol. 32, no. 5, pp. 1029–1040, Sep. 1994.

[11] J. Li, J. Chen, P. Wang, and O. Loffeld, "A coarse-to-fine autofocus approach for very high-resolution airborne stripmap SAR imagery," *IEEE Trans. Geosci. Remote Sens.*, vol. 56, no. 7, pp. 3814–3829, Jul. 2018.

[12] D. E. Wahl, P. H. Eichel, D. C. Ghiglia, and C. V. Jakowatz, "Phase gradient autofocus—A robust tool for high resolution SAR phase correction," *IEEE Trans. Aerosp. Electron. Syst.*, vol. 30, no. 3, pp. 827–835, Jul. 1994.

[13] J. R. Moreira, "A new method of aircraft motion error extraction from radar raw data for real time motion compensation," *IEEE Trans. Geosci. Remote Sens.*, vol. 28, no. 4, pp. 620–626, Jul. 1990.

[14] J. Guo, J. Chen, C. Li, and W. Yang, "An airborne multi-channel SAR imaging method with motion compensation," in *Proc. IEEE Int. Geosci. Remote Sens. Symp.*, 2019, pp. 8554–8557.

[15] Yan-Yang Liu, Z. Li, Zhi-Yong Suo, and Z. Bao, "A novel channel phase bias estimation method for spaceborne along-track multi-channel HRWS SAR in time-domain," in *Proc. IET Int. Radar Conf.*, 2013, pp. 1–4.

[16] J. Feng, C. Gao, Y. Zhang, and R. Wang, "Phase mismatch calibration of the multichannel SAR based on azimuth cross correlation," *IEEE Geosci. Remote Sens. Lett.*, vol. 10, no. 4, pp. 903–907, Jul. 2013.

[17] M. Shang, X. Qiu, B. Han, C. Ding, and Y. Hu, "Channel imbalances and along-track baseline estimation for the GF-3 azimuth multichannel mode," *Remote Sens.*, vol. 11, no. 11, p. 1297, May 2019, Art. no. 1297.

[18] Z. Wang, Y. Liu, Z. Li, G. Xu, and J. Chen, "Phase bias estimation for multichannel HRWS SAR based on Doppler spectrum optimisation," *Electron. Lett.*, vol. 52, no. 21, pp. 1805–1807, 2016.

[19] Y. Liu, Z. Li, T. Yang, and Z. Bao, "An adaptively weighted least square estimation method of channel mismatches in phase for multichannel SAR systems in azimuth," *IEEE Geosci. Remote Sens. Lett.*, vol. 11, no. 2, pp. 439–443, Feb. 2014.

[20] H. Gao, J. Chen, S. Quegan, W. Yang, and C. Li, "Parameter estimation and error calibration for multi-channel beam-steering SAR systems," *Remote Sens.*, vol. 11, no. 12, p. 1415, 2019, Art. no. 1415.

[21] Z. Li, Z. Bao, H. Wang, and G. Liao, "Performance improvement for constellation SAR using signal processing techniques," *IEEE Trans. Aerosp. Electron. Syst.*, vol. 42, no. 2, pp. 436–452, Apr. 2006.

[22] A. Liu, G. Liao, L. Ma, and Q. Xu, "An array error estimation method for constellation SAR systems," *IEEE Geosci. Remote Sens. Lett.*, vol. 7, no. 4, pp. 731–735, Oct. 2010.

[23] A. Liu, G. Liao, Q. Xu, and L. Ma, "An improved array-error estimation method for constellation SAR systems," *IEEE Geosci. Remote Sens. Lett.*, vol. 9, no. 1, pp. 90–94, Jan. 2012.

[24] L. Zhang, M. Xing, C. Qiu, and Z. Bao, "Adaptive two-step calibration for high resolution and wide-swath SAR imaging," *IET Radar, Sonar, Navigat.*, vol. 4, no. 4, pp. 548–559, Aug. 2010.

[25] S. X. Zhang, M. D. Xing, X. G. Xia, Y. Y. Liu, G. Rui, and B. Zheng, "A robust channel-calibration algorithm for multi-channel in azimuth HRWS SAR imaging based on local maximum-likelihood weighted minimum entropy," *IEEE Trans. Image Process.*, vol. 22, no. 12, pp. 5294–5305, Dec. 2013.

[26] C. Fang, Y. Liu, S. Ye, and W. Hou, "Space-variant channel phase bias calibration in airborne multichannel HRWS SAR imaging," in *Proc. China Int. SAR Symp.*, 2018, pp. 1–4.

[27] S. X. Zhang, M. D. Xing, X. G. Xia, L. Zhang, and Z. Bao, "Multichannel HRWS SAR imaging based on range-variant channel calibration and multi-Doppler-direction restriction ambiguity suppression," *IEEE Trans. Geosci. Remote Sens.*, vol. 52, no. 7, pp. 4306–4327, Jul. 2014.

[28] K. Raney, H. Runge, R. Bamler, I. Cumming, and F. H. Wong, "Precision SAR processing using chirp scaling," *IEEE Trans. Geosci. Remote Sens.*, vol. 32, no. 4, pp. 786–799, Jul. 1994.

Jiayi Guo (Graduate Student Member, IEEE) was born in Dezhou, China, in 1996. She received the B.S. degree, in 2018, from Shenyuan Honors College, Beihang University, Beijing, China, where she is currently working toward the Ph.D. degree in signal processing with the School of Electronics and Information Engineering.

Her research interests include multichannel SAR imaging and channel mismatch correction.

Jie Chen (Senior Member, IEEE) was born in Zhengzhou, China, in 1973. He received the B.S. and Ph.D. degrees in information and communication engineering from Beihang University, Beijing, China, in 1996 and 2002, respectively.

Since 2004, he has been an Associate Professor with the School of Electronics and Information Engineering, Beihang University. He was a Visiting Researcher with the School of Mathematics and Statistics, University of Sheffield, Sheffield, U.K., from 2009 to 2010, where he was involved in ionospheric effects on low-frequency space radars that measure forest biomass and ionospheric electron densities. Since 2011, he has been a Professor with the School of Electronics and Information Engineering, Beihang University. His research interests include multimodal remote-sensing data fusion, topside ionosphere exploration with spaceborne HF/VHF-synthetic aperture radar (SAR) system, high-resolution spaceborne SAR image formation, and SAR image quality enhancement.

Wei Liu (Senior Member, IEEE) received the B.Sc. and L.L.B. degrees from Peking University, Beijing, China, in 1996 and 1997, respectively, the M.Phil. degree from the University of Hong Kong, Hong Kong, in 2001, and the Ph.D. degree from the School of Electronics and Computer Science, University of Southampton, Southampton, U.K., in 2003.

He was a Postdoctoral Fellow with the Imperial College London, Kensington, U.K. Since 2005, he has been a Lecturer with the Department of Electronic and Electrical Engineering, University of Sheffield, Sheffield, U.K., where he became a Senior Lecturer. He has authored more than 200 journal and conference papers, three book chapters, and a research monograph about wideband beamforming: *Wideband Beamforming: Concepts and Techniques* (Wiley, 2010). His research interests include sensor array signal processing, blind signal processing, multirate signal processing, and their various applications in wireless communications, radar, sonar, satellite navigation, human–computer interface, and renewable energy exploitation.

Dr. Liu is an elected member of the Digital Signal Processing Technical Committee of the IEEE Circuits and Systems Society, the Sensor Array and Multichannel Signal Processing Technical Committee of the IEEE Signal Processing Society, and an Editorial Board Member of the *Journal Frontiers of Information Technology and Electronic Engineering.* He is currently an Associate Editor for the IEEE TRANSACTIONS ON SIGNAL PROCESSING and IEEE ACCESS.

Chunsheng Li received the Ph.D. degree in signal and information processing from the Beijing University of Aeronautics and Astronautics (now Beihang University), Beijing, China, in 1998.

Since 2005, he has been a Professor with the School of Electronics and Information Engineering, Beihang University. He has authored more than 100 journal and conference papers and four books. His research interests include analysis and simulation of synthetic aperture radar satellite, high-resolution image formation, and multimodal remote sensing data fusion.

Wei Yang (Associate Member, IEEE) was born in Hubei, China, in 1983. He received the M.S. and Ph.D. degrees in signal and information processing from Beihang University [previously known as Beijing University of Aeronautics and Astronautics (BUAA)], Beijing, China, in 2008 and 2011, respectively.

In 2005, he studied the inner calibration signal analysis in synthetic aperture radar (SAR) systems. From 2006 to 2010, he focused on the system performance analysis and signal processing of high-resolution and wide-swath mode in spaceborne SAR, including the multichannel terrain observation with progressive scan mode and the ScanSAR mode. Since 2011, he has been a Postdoctoral Researcher with the School of Electronics and Information Engineering, BUAA. His current research interests include ultrahigh-resolution spaceborne SAR image formation, modeling and data simulation, and novel techniques for spaceborne SAR systems.